Talanta 81 (2010) 1022–1027

Contents lists available at ScienceDirect

Talanta

journal homepage: www.elsevier.com/locate/talanta

# Rapid DNA electrochemical biosensing platform for label-free potentiometric detection of DNA hybridization

Meng Du, Tao Yang, Kui Jiao*

*Key Laboratory of Eco-chemical Engineering (Ministry of Education), College of Chemistry and Molecular Engineering, Qingdao University of Science and Technology, Qingdao 266042, China*

ARTICLE INFO

*Article history:*
Received 23 November 2009
Received in revised form 20 January 2010
Accepted 24 January 2010
Available online 1 February 2010

*Keywords:*
Sulfonated polyaniline
Layer-by-layer
DNA hybridization
Chronopotentiometry

ABSTRACT

This paper described a novel electrochemical DNA biosensor for rapid specific detection of nucleic acids based on the sulfonated polyaniline (SPAN) nanofibre and cysteamine-capped gold nanoparticle (CA-$G_{NP}$) layer-by-layer films. A precursor film of 3-mercaptopropionic acid (MPA) was firstly self-assembled on the Au electrode surface. CA-$G_{NP}$ was covalently deposited on the Au/MPA electrode to obtain a stable substrate. SPAN nanofibre and CA-$G_{NP}$ were alternately layer-by-layer assembled on the stable substrate by electrostatic force. Cyclic voltammetry was used to monitor the consecutive growth of the multilayer films by utilizing $[Fe(CN)_6]^{3-/4-}$ as the redox indicator. The (CA-$G_{NP}$/SPAN)$_n$ films showed satisfactory ability of electron transfer and excellent redox activity in neutral media. Negatively charged probe ssDNA was immobilized on the outer layer of the multilayer film (CA-$G_{NP}$) through electrostatic affinity. Chronopotentiometry and electrochemical impedance spectroscopy were employed to obtain the direct electrochemical readout for probe ssDNA immobilization and hybridization using $[Fe(CN)_6]^{3-/4-}$ in solution as the mediator. While electrochemical impedance spectroscopy led to the characterization of the electron-transfer resistance at the electrode, chronopotentiometry provided the total resistance at the interfaces of the modified electrodes. A good correlation between the total electrode resistances and the electron-transfer resistances at the conducting supports was found. Chronopotentiometry was suggested as a rapid transduction means (a few seconds). Based on the (CA-$G_{NP}$/SPAN)$_n$ films, the target DNA with 20-base could be detected up to $2.13 \times 10^{-13}$ mol/L, and the feasibility for the detection of base-mismatched DNA was also demonstrated.



## 1. Introduction

There is increased interest toward the application of conducting polymer-based nucleic acid sensors [1]. Among electrically conducting polymers, polyaniline (PANI) [2–7] has been the focus of much attention because of its unusual physical properties, improved processability, and potential industrial applications. Feng et al. [8] constructed gold nanoparticle/polyaniline nanotube membranes on the glassy carbon electrode for the electrochemical sensing of the immobilization and hybridization of DNA. The synergistic effect of the two kinds of nanomaterials could enhance dramatically the sensitivity for the DNA hybridization recognition. DNA sequence-specific of phosphinothricin acetyltransferase (PAT) gene existing in some transgenic crops was detected by electrochemical impedance spectroscopy (EIS). Zhang et al. [9] prepared a conductive interface for electrochemical label-free EIS detection of DNA hybridization by combining the strong adsorption ability of $Fe_2O_3$ microspheres to the DNA probes and excellent conductivity of self-doped polyaniline nanofibres (copolymer of aniline and *m*-aminobenzenesulfonic acid) on carbon ionic liquid electrode. The immobilization of the probe DNA on the surface of electrode and the sensitivity of DNA hybridization recognition were dramatically enhanced due to the unique synergistic effect of $Fe_2O_3$ microspheres, self-doped polyaniline nanofibres and ionic liquid.

Layer-by-layer (LBL) assembly is a simple and versatile technique for fabricating ultrathin films on solid substrates [10]. Knoll and coworkers [11] fabricated PANI/gold nanoparticle multilayer films obtained via the LBL technique. They found that the redox activity of PANI can also be shifted to neutral conditions by doping it with mercaptosuccinic-acid-capped gold nanoparticle instead of the normally used polyelectrolytes. The PANI/gold nanoparticle multilayer films could electrocatalyze the oxidation of nicotinamide adenine dinucleotide (NADH) and also be used to detect DNA hybridization by both EIS and surface plasmon enhanced fluorescence spectroscopy. Sulfonated polyaniline (SPAN), as one of the PANI derivatives, is the first reported self-doped water-soluble conducting PANI derivative [12]. The environmental and thermal stability of the parent PANI is further improved in SPAN [13]. Due

* Corresponding author. Tel.: +86 532 84855977; fax: +86 532 84023927.
*E-mail address:* kjiao@qust.edu.cn (K. Jiao).

0039-9140/$ – see front matter © 2010 Elsevier B.V. All rights reserved.
doi:10.1016/j.talanta.2010.01.053

to the introduction of acidic groups $-SO_3^-$ into the PANI chain, the conductivity of SPAN is independent of external protonation in a broad pH range. All these greatly promote its applicability in bioelectrochemistry. Gold nanoparticle is expected to be a good stabilization linker to SPAN in aqueous medium due to its high biocompatibility, good conductivity, and distinctive size-related electronic and optical behaviors [14].

EIS is a powerful method of analyzing the complex electrical resistance of a system and is sensitive to surface phenomena and changes of bulk properties [15]. However, it needs a tedious process requiring recording of the impedance features in a broad frequency domain (analysis time ca. 15–20 min), and cannot be applied for rapid biosensing. We wish to use chronopotentiometry (CP) as an electrochemical means that could rapidly detect DNA hybridization events. Willner and coworkers [16] introduced CP as an instantaneous electrochemical means that probes the resistance of the electrode/solution interface. They demonstrated that CP could provide useful basic information related to the changes in the resistance of the electrode occurring upon its modification. Their results highlighted the fact that the interfacial electron-transfer resistances derived from EIS were almost identical to the total electrode resistances extracted from CP. It indicated the powerful potential of CP for the application of rapid electrochemical biosensing.

Herein, we investigated the potential use of the LBL technique to create composite polymeric multilayer films that were both electronically conductive and catalytically active. SPAN nanofibre and CA-$G_{NP}$ LBL multilayer films $(CA\text{-}G_{NP}/SPAN)_n$ were prepared on the stable Au/MPA substrate. Results demonstrated that the $(CA\text{-}G_{NP}/SPAN)_n$ were very stable and showed excellent conductive activity in $[Fe(CN)_6]^{3-/4-}$ solution. In the $(CA\text{-}G_{NP}/SPAN)_n$, gold nanoparticle could stabilize the SPAN and greatly improve the redox activity of SPAN in neutral solution due to the unique synergistic effect of SPAN and gold nanoparticle. The immobilization and hybridization of DNA on the multilayer films were detected by both CP and EIS. In comparison, EIS was rather a time-consuming method than CP. We compared the results obtained by EIS and those derived from CP on the DNA sensing electrode. The biosensor based on $(CA\text{-}G_{NP}/SPAN)_3$ had high sensitivity, a relatively wide linear range from $1.0 \times 10^{-12}$ mol/L to $1.0 \times 10^{-7}$ mol/L and a powerful ability to discriminate the fully complementary target DNA from noncomplementary, single- or double-base-mismatched DNA.

## 2. Experimental

### 2.1. Apparatus and reagents

A CHI 660C electrochemical analyzer (Shanghai CH Instrument Company, China), which was in connection with a gold modified working electrode, a saturated calomel reference electrode (SCE) or a Ag/AgCl reference electrode and a platinum wire counter electrode, was used for the electrochemical measurements. The pH values of all solutions were measured by a model pHS-25 digital acidometer (Shanghai Leici Factory, China). Ultrapure water (resistivity: 18 MΩ cm) was prepared by aquapro ultrapure water system (Chongqing Yiyang Company, China).

The following reagents were all used as received: SPAN nanofibre [17] was kindly provided by College of Materials Science and Engineering, Qingdao University of Science and Technology (Fig. 1). Hydrogen tetrachloroaurate (III) tetrahydrate ($HAuCl_4 \cdot 4H_2O$, 99.9%, Sigma, St. Louis, MO, USA); CA (Sigma, St. Louis, MO, USA); $K_3[Fe(CN)_6]$ (Shanghai No. 1 Reagent Factory); $K_4[Fe(CN)_6]$ (Shanghai Heng Da Chemical Co. Ltd.); MPA (Sigma, St. Louis, MO, USA); 1-(3-dimethylaminopropyl)-3-ethylcarbodiimide hydrochloride (EDC, Sigma–Aldrich, USA); sodium dodecylsulfate (SDS). All the chemicals were of analytical grade and solutions were prepared with ultrapure water.

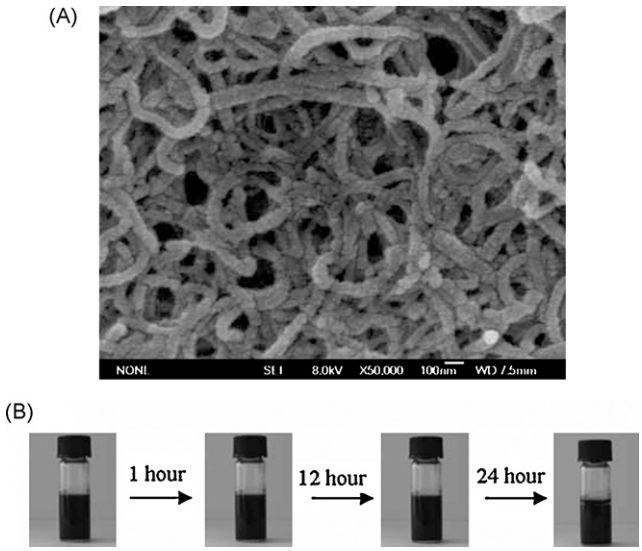


**Fig. 1.** The representative SEM images (A) and photographs (B) of SPAN nanofibre.

The 20-base oligonucleotides probe (ssDNA), its complementary sequence DNA (cDNA, target DNA, namely a 20-base fragment of the PAT gene sequence), single-base-mismatched DNA, double-base-mismatched DNA and noncomplementary DNA (ncDNA) were synthesized by Beijing SBS Gene Tech. Co. Ltd. Their base sequences are listed below:

Probe DNA (ssDNA): 5′-GCC ACA AAC ACC ACA AGA GT-3′.
Target DNA (cDNA): 5′-ACT CTT GTG GTG TTT GTG GC-3′.
Single-base-mismatched DNA: 5′-ACT CTG GTG GTG TTT GTG GC-3′.
Double-base-mismatched DNA: 5′-ACT CTG GTG GTG CTT GTG GC-3′.
ncDNA: 5′-CAT GGT TGA TCC GTT CGC TG-3′.

All oligonucleotides stock solutions were prepared using Tris–HCl solution (5.0 mmol/L Tris–HCl, 50.0 mmol/L NaCl, pH 7.0), and kept at 4 °C. More diluted solutions were obtained via diluting aliquot of the stock solutions with ultrapure water prior to use. The hybridization solution was diluted with 2× SSC (pH 7.0), which consists of 0.30 mol/L NaCl and 0.03 mol/L sodium citrate tribasic dihydrate ($C_6H_5Na_3O_7 \cdot 2H_2O$).

### 2.2. Cysteamine-capped gold nanoparticles synthesis

The water-dispersible cysteamine-capped gold nanoparticles were prepared following Kimura's method [18], but with an equal molar ratio of $HAuCl_4$ and cysteamine. In brief, in a 500-mL three neck round-bottom flask, 1.25 mmol $HAuCl_4 \cdot 4H_2O$ in 5 mL ultrapure water and 1.25 mmol CA in 245 mL ultrapure water were mixed and vigorously stirred for 30 min at room temperature. A freshly prepared 12.5 mmol $NaBH_4$ in 25 mL water was added into the above mixture drop by drop at a rate of 60–80 drops/min, and finished in ca. 5 min. After further stirring for 1 h, the precipitate was collected and washed by a repeated centrifugation–ultrasonic dispersion process in mixed methanol/$H_2O$ and finally dried in a vacuum. The main product was collected as 280 mg powder. The dipping solution was freshly prepared by redispersing the powder in ultrapure water at a concentration of 0.05 mg/mL.

### 2.3. Buildup of (CA-$G_{NP}$/SPAN)$_n$

The gold electrode was cleaned by immersing it in a 3:1 mixture of concentrated sulfuric acid and 30% hydrogen peroxide (piranha solution) for about 5 min, subsequently washed thoroughly with ultrapure water. The electrode was polished with 0.3 μm and 0.05 μm α-$Al_2O_3$, respectively, on a polishing pad (Buehler), followed by sonicated thoroughly in ultrapure water for 10 min. Finally, the electrode was cleaned electrochemically by cycling between −0.4 V and 1.5 V versus Ag/AgCl electrode in a 0.02 mol/L $H_2SO_4$ solution at a scan rate 100 mV/s until reproducible cyclic voltammograms at a clean gold electrode were obtained. Freshly cleaned gold electrode was immersed in an ethanol solution of MPA (5 mmol/L) for 12 h. The MPA modified electrode was immersed in a phosphate buffer solution (PBS, pH 7.0) of EDC (1.0 mmol/L) for 0.5 h. After that, the electrode was immersed in the CA-$G_{NP}$ solution, and the electrodeposition of CA-$G_{NP}$ was carried out at −1.5 V (vs. SCE) for 200 s. The electrode was then immersed in a PBS (pH 6.0) buffer of SPAN (1.0 g/L) for 0.5 h. Every assembly step was followed by a washing step with ultrapure water. The second layer of CA-$G_{NP}$ and SPAN was assembled with the same processes. Alternating layers of positively charged CA-$G_{NP}$ and negatively charged SPAN were deposited on the electrode surface (terminated layer by CA-$G_{NP}$). All above solutions were prepared freshly prior to use.

### 2.4. Immobilization and hybridization of probe ssDNA on modified gold electrode and electrochemical detection

The amino groups of CA-$G_{NP}$ on the electrode surface could form an electrostatic affinity with the phosphate skeleton of DNA molecule to immobilize the DNA probe. The multilayer films modified gold electrode was immersed in 2.0 ml Tris–HCl buffer solution (pH 7.0) containing $1.0 \times 10^{-7}$ mol/L ssDNA at 35 °C for 30 min to obtain a probe ssDNA-modified gold electrode. After that, the electrode was washed with ultrapure water before hybridization.

Hybridization reaction was conducted by immersing the DNA probe-modified gold electrode in a hybridization solution (2× SSC buffer, pH 7.0) containing the target DNA at 40 °C for 30 min. The electrode was washed with SDS solution to remove the unhybridized DNA.

The cyclic voltammetric measurement was performed in 1.0 mmol/L $K_3[Fe(CN)_6]/K_4[Fe(CN)_6]$ solution containing 0.1 mol/L KCl at the scan rate of 100 mV/s. The chronopotentiometry was recorded in 2.0 mmol/L $K_3[Fe(CN)_6]/K_4[Fe(CN)_6]$ solution containing 0.1 mol/L KCl with cathodic current $5.0 \times 10^{-4}$ A. Electrochemical impedance spectroscopic measurement of 2.0 mmol/L $K_3[Fe(CN)_6]/K_4[Fe(CN)_6]$ was performed with 0.1 mol/L KCl as the supporting electrolyte. The AC voltage amplitude was 5 mV and the voltage frequencies ranged from 10 kHz to 0.01 Hz. The applied potential was 0.172 V.

## 3. Results and discussion

### 3.1. LBL self-assembly of SPAN and CA-$G_{NP}$

To investigate the conductive effect of SPAN, cyclic voltammetry was tested for the films using $[Fe(CN)_6]^{3-/4-}$ as an electroactive probe. Fig. 2 shows the cyclic voltammograms of 1.0 mmol/L $[Fe(CN)_6]^{3-/4-}$ at (a) bare Au electrode; (b) the MPA modified electrode, (c) gold nanoparticles modified electrode and (d–f) different number of CA-$G_{NP}$/SPAN bilayer electrodes. As could be seen, when compared the SPAN modified electrodes (curves d–f) with the non-SPAN modified electrodes (curves a–c), the SPAN modified electrodes exhibited the larger background current. The LBL assembly process of the (CA-$G_{NP}$/SPAN)$_n$ multilayer films was also shown

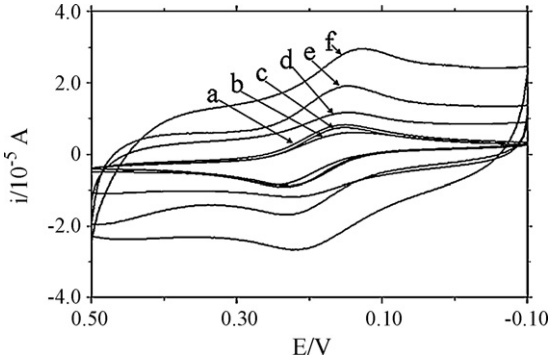


**Fig. 2.** Cyclic voltammograms of 1.0 mmol/L $[Fe(CN)_6]^{3-/4-}$ in 0.1 mol/L KCl at (a) bare Au, (b) Au/MPA, (c) Au/MPA/CA-$G_{NP}$, (d) Au/MPA/(CA-$G_{NP}$/SPAN), (e) Au/MPA/(CA-$G_{NP}$/SPAN)$_2$ and (f) Au/MPA/(CA-$G_{NP}$/SPAN)$_3$.

in Fig. 2. The gradual increase of the background current with the $n$ value indicated a progressive deposition of SPAN and CA-$G_{NP}$ layers onto the gold substrate in each cycle (curves d–f). However, the increase of the peak current at the SPAN modified electrodes was not obvious due to the large background current. It indicated that electrode modified with SPAN nanofibres had a larger electrode effective surface area than non-SPAN modified electrode or bare electrode [19].

### 3.2. Properties of (CA-$G_{NP}$/SPAN)$_n$ multilayer films in neutral solution

The (CA-$G_{NP}$/SPAN)$_n$ films provided a favorable microenvironment to enhance the electron transfer on the electrode (Fig. 3). A redox peak with the formal potential being around 0.09 V was found for different bilayers of CA-$G_{NP}$/SPAN in Britton–Robinson (B–R, pH 7.0) buffer solution. This redox peak is the redox process normally found for SPAN under neutral conditions [20]. Both reduction and oxidation peaks grew gradually with the number of CA-$G_{NP}$/SPAN bilayers ($n$) up to 3, and then reached the stable values with the further increase of $n$ value. The corresponding peak-to-peak separation also decreased with the growth of multilayer films until $n = 3$. We also studied the stability of the (CA-$G_{NP}$/SPAN)$_n$ multilayer films. For example, after placed in B–R buffer (pH 7.0) for 40 h, the peak currents of (CA-$G_{NP}$/SPAN)$_3$ films decreased by about 10%, and then no further decrease was observed for at least 10 days. In the (CA-$G_{NP}$/SPAN)$_3$ films, the two components formed an open and disordered structure, which facilitated both the effective doping of SPAN and the fast charge transfer. Moreover, the gold nanoparticle might also help the charge transfer across the film. This excellent

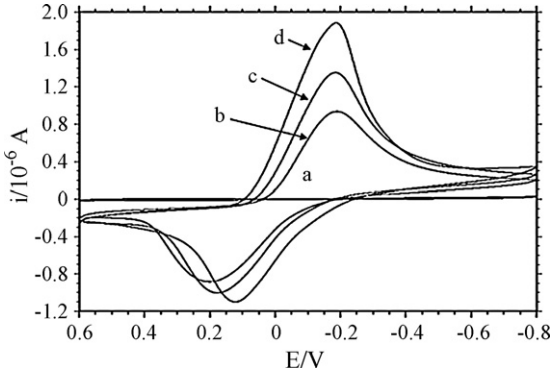


**Fig. 3.** Cyclic voltammograms of (a) Au/MPA/CA-$G_{NP}$, (b) Au/MPA/(CA-$G_{NP}$/SPAN), (c) Au/MPA/(CA-$G_{NP}$/SPAN)$_2$ and (d) Au/MPA/(CA-$G_{NP}$/SPAN)$_3$ recorded in B–R solution (pH 7.0). Scan rate: 100 mV/s.

electroactivity and stability of the $(CA\text{-}G_{NP}/SPAN)_n$ films in neutral pH environment offered interesting opportunities for applications in biosensors [21,22].

### 3.3. Analytical performance of the DNA biosensor

#### 3.3.1. CP and EIS studies on immobilization and hybridization of DNA

The probe DNA immobilization and hybridization on the $Au/MPA/(CA\text{-}G_{NP}/SPAN)_3/CA\text{-}G_{NP}$ electrode were monitored using CP and EIS. CP is an electrochemical technique that applies a constant and controlled current between the working electrode and auxiliary electrode, while the potential between two electrodes is altered to retain the desired current value. It is a rapid detection method and can easily be applied to follow the modification events on the electrode surface. The total electrode resistance ($R'$) was given by Eq. (1), where $I$ is the set constant current, $\eta$ is the overpotential on the electrode, which will relate to the change in the electrode resistance.

$$R' = \frac{\eta}{I} \quad (1)$$

A limitation should be mentioned upon the application of chronopotentiometry as an electrochemical method to analyze interface properties of layered-modified electrodes. The total electrode resistances do not coincide with the electron-transfer resistances ($R_{et}$) and the comparison of these values needs to be made with caution. While the total electrode resistances correspond to the entire current flux at the electrode, the electron-transfer resistances correspond only to the Faradaic current at the electrode interface. Thus, in the chronopotentiometric experiment, the non-Faradaic current originating from the double-layer charging always affects the electrode resistance. At high concentrations of the redox probe ($>10^{-3}$ mol/L) the double-layer charging current is negligible as compared to the Faradaic current [23]. Under these conditions, it is expected that $R' \approx R_{et}$. Furthermore, the double-layer charging current increases with the potential applied onto the electrode. Thus, at high overpotential values, resulting at certain modifications of the electrode, deviations between the total electrode resistances derived from CP and the electron-transfer resistances determined by EIS, may be observed, even at high concentrations of the redox probe.

Fig. 4A displays the CP responses of 2.0 mmol/L $[Fe(CN)_6]^{3-/4-}$ obtained at (a) $Au/MPA/(CA\text{-}G_{NP}/SPAN)_3/CA\text{-}G_{NP}$, (b) $Au/MPA/(CA\text{-}G_{NP}/SPAN)_3/CA\text{-}G_{NP}$/ssDNA and (f) $Au/MPA/(CA\text{-}G_{NP}/SPAN)_3/CA\text{-}G_{NP}$/dsDNA (hybridization with cDNA). The $Au/MPA/(CA\text{-}G_{NP}/SPAN)_3/CA\text{-}G_{NP}$ electrode exhibited a low $\eta$ (ca. 24 mV), which was translated to the $R'$ value corresponding to ca. 48 Ω. Upon the ssDNA immobilization and hybridization on the $Au/MPA/(CA\text{-}G_{NP}/SPAN)_3/CA\text{-}G_{NP}$ electrode a successive increase in the $\eta$ value was observed. These enhanced $\eta$ values were attributed to the electrostatic repulsion of the negatively charged redox indicator by negatively charged DNA. The $\eta$ values of curve b and f were 590 mV and 1130 mV, respectively. The corresponding $R'$ values were 1.18 kΩ and 2.26 kΩ, respectively. Every CP measurement was finished within 30 s, indicating CP was a rapid method. Fig. 4B shows the Nyquist diagrams of 2.0 mmol/L $[Fe(CN)_6]^{3-/4-}$ at (a) $Au/MPA/(CA\text{-}G_{NP}/SPAN)_3/CA\text{-}G_{NP}$, (b) $Au/MPA/(CA\text{-}G_{NP}/SPAN)_3/CA\text{-}G_{NP}$/ssDNA and (f) $Au/MPA/(CA\text{-}G_{NP}/SPAN)_3/CA\text{-}G_{NP}$/dsDNA (hybridization with cDNA). The semicircle diameter in the impedance spectrum equals to $R_{et}$. The $R_{et}$ value of $Au/MPA/(CA\text{-}G_{NP}/SPAN)_3/CA\text{-}G_{NP}$ was ca. 60 Ω, while that of ssDNA-modified electrode was ca. 1.14 kΩ. The change of the $R_{et}$ value was strong proof that the ssDNA had been immobilized on the $Au/MPA/(CA\text{-}G_{NP}/SPAN)_3/CA\text{-}G_{NP}$ surface. The negatively charged phosphate backbone of the ssDNA prevented

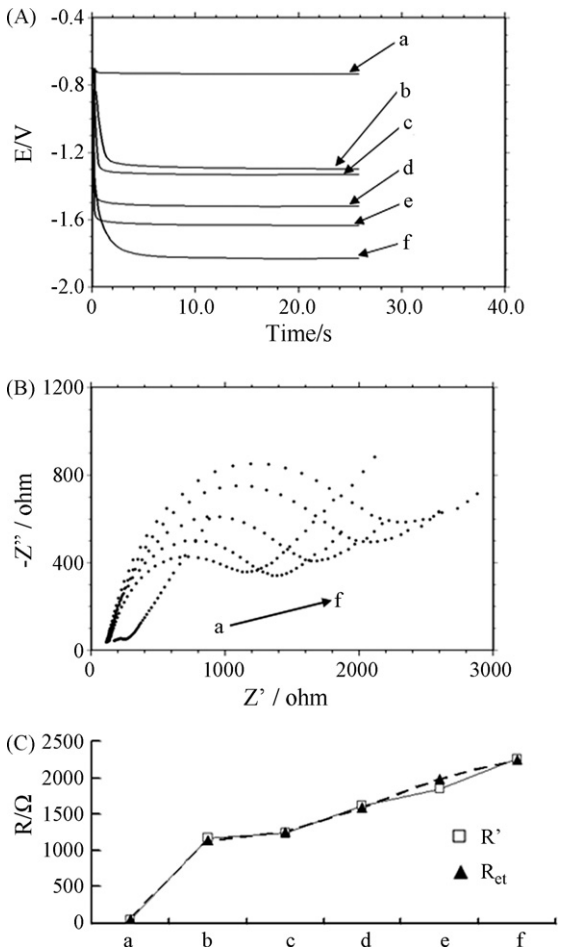


**Fig. 4.** (A) Chronopotentiometric curves and (B) Nyquist diagrams of 2.0 mmol/L $[Fe(CN)_6]^{3-/4-}$ recorded at (a) $Au/MPA/(CA\text{-}G_{NP}/SPAN)_3/CA\text{-}G_{NP}$, (b) $Au/MPA/(CA\text{-}G_{NP}/SPAN)_3/CA\text{-}G_{NP}$/ssDNA, (c) $Au/MPA/(CA\text{-}G_{NP}/SPAN)_3/CA\text{-}G_{NP}$/dsDNA (hybridization with ncDNA), (d) the electrode hybridized with double-base-mismatched DNA, (e) the electrode hybridized with single-base-mismatched DNA and (f) the electrode hybridized with cDNA (concentrations of PAT gene sequence-specific: $1.0 \times 10^{-7}$ mol/L). (C) The comparison of total electrode resistance ($R'$) derived from (A) and electron-transfer resistance ($R_{et}$) derived from (B).

$[Fe(CN)_6]^{3-/4-}$ from reaching the electrode surface, leading to a much larger $R_{et}$ value. After hybridization of the DNA probe with cDNA, the $R_{et}$ value increased greatly to ca. 2.26 kΩ (curve f). Obviously, the CP and EIS measurements all confirmed that the ssDNA-modified electrode could successfully detect the target DNA. The results showed that the total electrode resistances extracted from the CP measurements were very close to the electron-transfer resistances obtained from the EIS.

#### 3.3.2. Optimization of DNA immobilization and hybridization

In the process of electrode modification, the immobilization of the ssDNA on the $(CA\text{-}G_{NP}/SPAN)_n$ multilayer films was a crucial step. The ssDNA immobilization temperature and time directly affected the immobilization amount. The ssDNA was immobilized at different temperature, such as 20 °C, 25 °C, 30 °C, 35 °C, 40 °C, and 45 °C, and the CP measurements at the electrode after every DNA immobilization were, respectively, recorded. The results showed that the overpotential difference ($\Delta\eta$) between ssDNA-modified electrode and the multilayer film-modified electrode increased with the positive shift of the temperature from 20 °C to 35 °C, and then reached a constant level beyond 35 °C (Fig. 5A). Therefore, 35 °C was selected for the immobilization of ssDNA in our experiments. The ssDNA was immobilized at 35 °C for different time

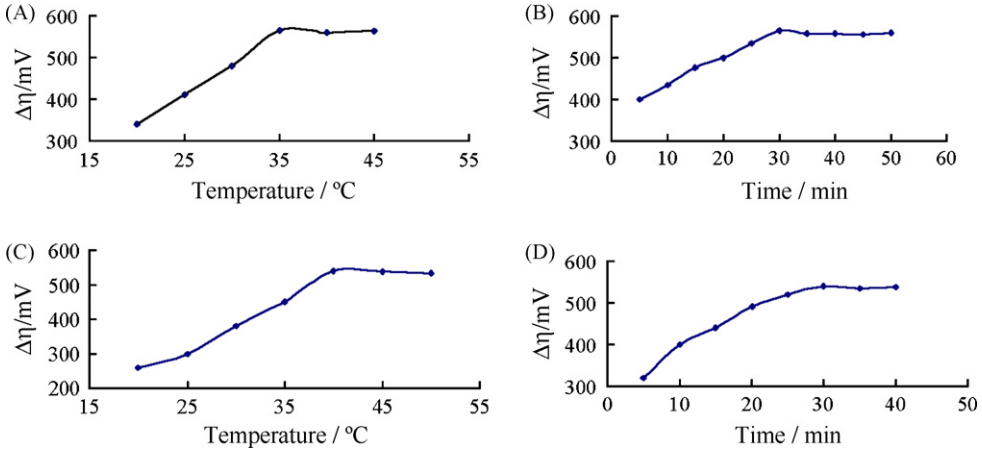


**Fig. 5.** Influence of immobilization temperature (A) and time (B) on $\Delta\eta$ between ssDNA-modified electrode and the multilayer film-modified electrode. Influence of hybridization temperature (C) and time (D) on $\Delta\eta$ between the hybridized electrode and the ssDNA-modified electrode.

from 5 min to 50 min, and the results indicated that the $\Delta\eta$ rose gradually at first (up to 30 min) and then reached a constant level (Fig. 5B). 30 min was used for the optimal immobilization time in experiments.

The hybridization temperature and time had important effect on the hybridization reaction. The ssDNA-modified electrode was hybridized by immersing it in a hybridization solution containing $1.0 \times 10^{-7}$ mol/L target DNA at different temperature, such as 20 °C, 25 °C, 30 °C, 35 °C, 40 °C, 45 °C and 50 °C, for different time. The $\Delta\eta$ between the hybridized electrode and the ssDNA-modified electrode reached the maximum value at the hybridization temperature of 40 °C, which showed that the highest hybridization efficiency was obtained at 40 °C (Fig. 5C). As a result, 40 °C was selected in this work. With the hybridization time from 5 min to 40 min, the $\Delta\eta$ increased dramatically with prolonging the hybridization time until 30 min and then tended to a stable level (Fig. 5D). So a hybridization time of 30 min was adopted in the experiments.

### 3.3.3. *Selectivity and sensitivity of DNA hybridization recognition*

The selectivity of this DNA biosensor was investigated by using the DNA probe to hybridize with different DNA sequences related to PAT gene. The potentiometric responses were also given in Fig. 4A. The curve b was the CP signal at the Au/MPA/(CA-$G_{NP}$/SPAN)$_3$/CA-$G_{NP}$/ssDNA. After hybridization of the ssDNA with the cDNA (f), the overpotential increased obviously, suggesting that hybrids (dsDNA) were formed at the electrode. The increase of the overpotential was negligible after the DNA probe was hybridized with the ncDNA (c), indicating that the hybridization reaction was not achieved. After the ssDNA was hybridized with the single-base-mismatched DNA sequence (e) or double-base-mismatched DNA sequence (d), the increase of the overpotential was much smaller than that obtained from the hybridization with the cDNA (f). The single-base-mismatched and double-base-mismatched DNA sequences could also be recognized via comparing the increase of the overpotential. The results demonstrated that this DNA biosensor displayed very high selectivity for the hybridization detection. Fig. 4B shows Nyquist plots of impedance for the ssDNA-modified electrode and different hybridized electrodes. It could be seen that the semicircle diameters of EIS increase from curve b to curve f, implying an enhancement in the interfacial electron-transfer resistance. Fig. 4C plots $R_{et}$ derived from the impedance measurements and $R'$ derived from the CP measurements at the same level. One might see that the values of $R'$ and $R_{et}$ were almost the same. It demonstrated that non-Faradaic double-layer charging current has little effect on the interfacial electron-transfer resistance in this system.

The $R'$ differences ($\Delta R'$) between the ssDNA-modified electrode and the hybridized electrode derived from the CP measurements and the $R_{et}$ differences ($\Delta R_{et}$) between the ssDNA-modified electrode and the hybridized electrode derived from the EIS measurements were both used to be the measurement signal for quantitative analysis of the PAT gene target sequence. The concentration of the PAT gene target sequence in the hybridization solution was changed from $1.0 \times 10^{-12}$ mol/L to $1.0 \times 10^{-7}$ mol/L, and the results from CP and EIS were shown in Fig. 6A and B, respectively. In Fig. 6C, the $\Delta R'$ value was linear with the logarithm of the PAT gene target sequence concentration in the range of $1.0 \times 10^{-12}$ mol/L to $1.0 \times 10^{-7}$ mol/L with a correlation coefficient ($R$) of 0.9899. The regression equation was $\Delta R' = 177.14 \lg C + 2256.2$ ($C$, mol/L; $\Delta R'$, Ω), and a detection limit of $2.13 \times 10^{-13}$ mol/L could be estimated using $3\sigma$ (where $\sigma$ was the R.S.D. of the blank solution, $n = 11$). The $\Delta R_{et}$ value was also linear with the logarithm of the PAT gene target sequence concentrations in the range of $1.0 \times 10^{-12}$ mol/L to $1.0 \times 10^{-7}$ mol/L with a correlation coefficient ($R$) of 0.9931. The regression equation was $\Delta R_{et} = 204.91 \lg C + 2562.4$ ($C$, mol/L; $\Delta R_{et}$, Ω), and a detection limit of $2.34 \times 10^{-13}$ mol/L could be estimated using $3\sigma$. It can be seen that the detection limit derived from the CP method is almost the same with that from the EIS. Moreover, the CP method is much more rapid and its manipulation is more convenient than the EIS method for the detection of DNA sequence-specific.

### 3.3.4. *Stability, reproducibility and regeneration ability of the biosensor*

The ssDNA-modified electrode was immersed in 2.0 mL 0.1 mol/L NaOH solution for 60 min. Any decrease of the electrode overpotential was not observed when the electrode was recorded in 2.0 mmol/L $[Fe(CN)_6]^{3-/4-}$ after the immersion. The same experiments using 0.1 mol/L HCl, Tris–HCl buffer (pH 7.0) and 2× SSC solution (pH 7.0), respectively, replacing 0.1 mol/L NaOH solution, were conducted; also, no overpotential decrease was observed. The above results showed that the probe Au/MPA/(CA-$G_{NP}$/SPAN)$_3$/CA-$G_{NP}$/ssDNA was of high stability and could be applied for the hybridization detection.

The reproducibility of the proposed method was investigated by detecting $1.0 \times 10^{-10}$ mol/L target DNA sequence. The $\Delta\eta$ values between at the probe ssDNA-modified electrode and at the hybridized electrode for five multiplayer membrane-modified electrodes parallel-prepared under the same conditions were 238 mV, 234 mV, 232 mV, 228 mV and 226 mV. The R.S.D. was 2.82% ($n = 5$). It indicated that a satisfactory reproducibility could be obtained by this DNA biosensor.

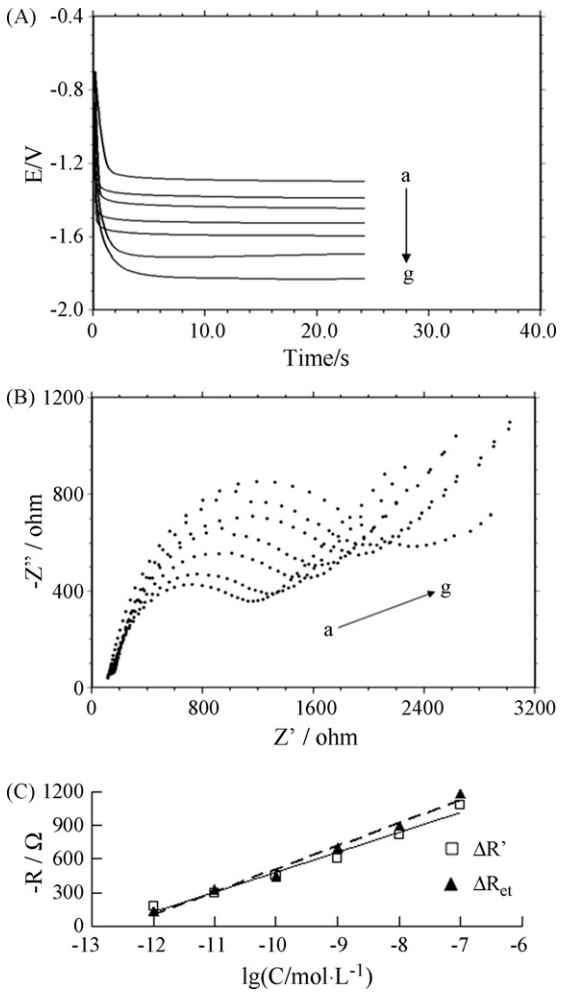


**Fig. 6.** (A) Chronopotentiometric curves and (B) Nyquist diagrams of 2.0 mmol/L $[Fe(CN)_6]^{3-/4-}$ recorded at (a) Au/MPA/$(CA\text{-}G_{NP}/SPAN)_3$/CA-$G_{NP}$/ssDNA, and after hybridization with different concentrations of PAT gene sequence (mol/L): (b) $1.0\times10^{-12}$, (c) $1.0\times10^{-11}$, (d) $1.0\times10^{-10}$, (e) $1.0\times10^{-9}$, (f) $1.0\times10^{-8}$ and (g) $1.0\times10^{-7}$. (C) The comparison for plots of $\Delta R'$ and $\Delta R_{et}$ versus logarithm of PAT gene fragment concentration.

The dsDNA on the hybridized electrode was hot denatured by immersing the electrode in boiling water for 10 min, and then cooled down rapidly with an ice salt bath, followed by rinsing the electrode with ultrapure water. The CP curves of $[Fe(CN)_6]^{3-/4-}$ at the regenerated ssDNA-modified electrode and its hybridized electrode were recorded. The results indicated that the two $\eta$ values at the probe electrode and the hybridized electrode and their $\Delta\eta$ value were almost the same as those obtained in the first experiment. Repetitive experiments showed that the DNA biosensor could be reproduced for five times without losing its sensitivity, exhibiting the fine regeneration ability of this DNA biosensor.

## 4. Conclusions

In this work, an efficient DNA immobilization platform based on the $(CA\text{-}G_{NP}/SPAN)_n$ multilayers was developed by LBL technique. $[Fe(CN)_6]^{3-/4-}$ was used as electroactive species to gain insight into the mechanism of charge transport through $(CA\text{-}G_{NP}/SPAN)_n$ multilayers. $(CA\text{-}G_{NP}/SPAN)_n$ films displayed nice electrochemical properties because the conductive SPAN played a significant role in electron transfer in the films with underlying electrodes. The DNA immobilization and hybridization were monitored with label-free CP and EIS strategies. In comparison, CP was a faster method than EIS. The results demonstrated that the interfacial electron-transfer resistances derived from EIS were almost identical to the total electrode resistances extracted from CP, and that these values correlated nicely with the DNA hybridization events. It was found that the biosensor discriminated against mismatched nucleic acid samples of similar lengths. The CP-based DNA biosensor based on the $(CA\text{-}G_{NP}/SPAN)_n$ multiplayer films was satisfactorily used for the qualitative detection of the PAT gene.

## Acknowledgements

This project was supported by the National Natural Science Foundation of China (Nos. 20635020, 20805025 and 20975057), Doctoral Foundation of the Ministry of Education of China (No. 20060426001) and the Natural Science Foundation of Qingdao City (No. 09-1-3-25-jch).

## References

[1] H. Peng, L.J. Zhang, C. Soeller, J. Travas-Sejdic, Biomaterials 30 (2009) 2132–2148.
[2] K. Arora, N. Prabhakar, S. Chand, B.D. Malhotra, Biosens. Bioelectron. 23 (2007) 613–620.
[3] K. Arora, N. Prabhakar, S. Chand, B.D. Malhotra, Anal. Chem. 79 (2007) 6152–6158.
[4] Y. Ma, J. Zhang, G. Zhang, H. He, J. Am. Chem. Soc. 126 (2004) 7097–7101.
[5] L. Liang, J. Liu, J. Windisch, G.J. Exarhos, Y. Lin, Angew. Chem. Int. Ed. 41 (2002) 3665–3668.
[6] H. Chang, Y. Yuan, N. Shi, Y. Guan, Anal. Chem. 79 (2007) 5111–5115.
[7] Z. Gao, S. Rafea, L.H. Lim, Adv. Mater. 19 (2007) 602–606.
[8] Y.Y. Feng, T. Yang, W. Zhang, C. Jiang, K. Jiao, Anal. Chim. Acta 616 (2008) 144–151.
[9] W. Zhang, T. Yang, X. Li, D.B. Wang, K. Jiao, Biosens. Bioelectron. 25 (2009) 428–434.
[10] W. Zhao, J.J. Xu, H.Y. Chen, Electroanalysis 18 (2006) 1737–1748.
[11] S. Tian, J. Liu, T. Zhu, W. Knoll, Chem. Mater. 16 (2004) 4103–4108.
[12] A. MacDiarmid, A. Epstein, Synth. Met. 65 (1994) 103–116.
[13] J. Yue, A. Epstein, Z. Zhong, P. Gallogher, A. MacDiarmid, Synth. Met. 41 (1991) 765–768.
[14] M.C. Daniel, D. Astruc, Chem. Rev. 104 (2004) 293–346.
[15] F. Lisdat, D. Schafer, Anal. Bioanal. Chem. 391 (2008) 1555–1567.
[16] L. Alfonta, A. Bardea, O. Khersonsky, E. Katz, I. Willner, Biosens. Bioelectron. 16 (2001) 675–687.
[17] C.Q. Zhang, G.C. Li, H.R. Peng, Mater. Lett. 63 (2009) 592–594.
[18] S. Chen, K. Kimura, Langmuir 15 (1999) 1075–1082.
[19] N.N. Zhu, Z. Chang, P.G. He, Y.Z. Fang, Electrochim. Acta 51 (2006) 3758–3762.
[20] S.A. Kumar, S.M. Chen, Sens. Actuators B: Chem. 123 (2007) 964–977.
[21] L. Zhang, X. Jiang, L. Niu, S.J. Dong, Biosens. Bioelectron. 21 (2006) 1107–1115.
[22] R. Mažeikienė, G. Niaura, A. Malinauskas, Electrochim. Acta 51 (2006) 5761–5766.
[23] A.J. Bard, L.R. Faulkner, Electrochemical Methods: Fundamentals and Applications, second edition, John Wiley & Sons, Inc., 2001.